PCCP

Accepted Manuscript

This is an *Accepted Manuscript*, which has been through the Royal Society of Chemistry peer review process and has been accepted for publication.

Accepted Manuscripts are published online shortly after acceptance, before technical editing, formatting and proof reading. Using this free service, authors can make their results available to the community, in citable form, before we publish the edited article. We will replace this *Accepted Manuscript* with the edited and formatted *Advance Article* as soon as it is available.

You can find more information about *Accepted Manuscripts* in the **Information for Authors**.

Please note that technical editing may introduce minor changes to the text and/or graphics, which may alter content. The journal's standard **Terms & Conditions** and the **Ethical guidelines** still apply. In no event shall the Royal Society of Chemistry be held responsible for any errors or omissions in this *Accepted Manuscript* or any consequences arising from the use of any information it contains.

Journal Name

COMMUNICATION

UV absorption probing of the conformer-dependent reactivity of a Criegee intermediate CH₃CHOO

Leonid Sheps,*[a] Ashley M. Scully,[b] and Kendrew Au[a]

We measure the UV absorption spectrum of a Criegee intermediate acetaldehyde oxide, CH₃CHOO, using time-resolved broadband cavity-enhanced spectrometry. We separate the spectra of the two possible structural isomers, *syn*- and *anti*-CH₃CHOO, based on their different reactivity towards H₂O and SO₂. Despite significant overlap, the spectra of the two conformers are sufficiently separated to allow direct conformer-specific probing of the reactions of CH₃CHOO with other important tropospheric species.

One of the primary pathways for the destruction of alkenes in the Earth's troposphere is reaction with ozone, which generates carbonyl oxides, known as Criegee intermediates (CI),[1] as shown in Scheme 1. When formed this way, CI are initially highly excited and quickly undergo collisional stabilization, dissociate, or convert to more stable isomers.[2-5] The reactivity of stabilized CI has long been a subject of interest because of their importance in ozonolysis and in atmospheric chemistry.[6-8] Yet, until recently no CI species had ever been directly observed experimentally and our understanding of their chemistry came from indirect studies based on end product analysis in the presence of competing kinetic pathways.

Scheme 1. Production of Criegee intermediates in ozonolysis of alkenes

However, in 2008 Taatjes and co-workers reported the first detection of CI[9] by photoionization mass spectrometry (PIMS); in 2012 the same group introduced an alternative means of CI formation in the gas phase[10] by photolysis-initiated reactions of iodoalkyl radicals with O₂ (Scheme 2). These nearly thermoneutral reactions offer a reliable method of generating high concentrations of stabilized Criegee intermediates, which has enabled rapid progress in our understanding of CI structure and reactivity. The simplest CI, CH₂OO, has been characterized by microwave,[11] IR,[12] and UV spectroscopy,[13-15] photodissociation dynamics studies,[16] and high-level quantum chemical calculations.[17] Spectroscopic studies are being extended to more complex methyl- and ethyl-substituted CI species: CH₃CHOO, (CH₃)₂COO, and CH₃CH₂CHOO have been studied by UV spectroscopy,[18-20] and there is also a report of a microwave spectrum of CH₃CHOO.[21]

Scheme 2. Production of Criegee intermediates by reaction of iodoalkyl radicals with O₂ (using CH₃CHOO as an example).

Kinetic studies of CI reactivity are also becoming possible using direct CI detection by PIMS[22,23] or optical detection of reaction products.[24,25] Such studies of CI reactions with key atmospheric species (H₂O, SO₂, NOₓ and others)[10,22,23] have led to significant improvements in previously assumed reaction rate coefficients – in some cases by orders of magnitude. In addition, our group recently showed that the intense UV absorption of CH₂OO is also an excellent direct probe of reaction kinetics. We used time-resolved UV spectroscopy to study the reactions of CH₂OO with SO₂[14] and with carboxylic acids;[26] others have since applied the same method to the reaction of CH₂OO with alkenes.[27]

Scheme 3   *anti*-CH₃CHOO   *syn*-CH₃CHOO

In contrast to CH₂OO, the next larger CI (CH₃CHOO, acetaldehyde oxide) has two possible conformers, *syn*- and *anti*-CH₃CHOO, shown in Scheme 3. This structural motif, which is representative of other CI with a single substituent alkyl group,[8] leads to complex conformer-dependent reactivity. Computational studies indicate that *syn*-CH₃CHOO is significantly less reactive than *anti*-CH₃CHOO towards, e.g., H₂O[2] and alkenes,[28] due to the electronic interactions and steric hindrance of the methyl group. Instead, the proximity of

the methyl group to the O-O moiety in *syn*-CH$_3$CHOO facilitates H transfer to the terminal O atom followed by OH elimination.

Motivated by its importance as a prototypical CI with a single alkyl substituent, we present here the UV absorption spectrum of acetaldehyde oxide, which includes resolved contributions from *syn*- and *anti*-CH$_3$CHOO. The difference in the UV spectra of the two conformers aids our understanding of the electronic structure and photochemistry of CH$_3$CHOO. In addition, our results enable direct conformer-specific probing of CH$_3$CHOO kinetics by time-resolved UV absorption spectroscopy. This probe technique can be a powerful complement to PIMS and in some cases can offer important advantages such as greater sensitivity.

Acetaldehyde oxide was produced as shown in Scheme 2. Pulsed 266-nm laser photolysis of CH$_3$CHI$_2$ generates CH$_3$CHI radicals, which react with an excess of O$_2$ in He bath gas at room temperature and a total pressure of 5 – 20 Torr. The experiments were performed using a recently constructed time-resolved cavity-enhanced absorption spectrometer that has already been used to measure the absorption spectrum of CH$_2$OO.[14] Briefly, a slow-flow chemical reactor is integrated into a broadband optical cavity, operating over the spectral range 300 – 450 nm for the present study. A Xe lamp provides continuous broadband probe radiation, and the effective path length in the reactor/cavity varies from 40 – 70 m, depending on the wavelength. The transient absorption spectra are acquired by a custom-built spectrometer, which captures the time evolution of the entire probe spectrum for every photolysis laser shot. The simultaneous broadband transient absorption probing is crucial in interpreting the kinetic measurements of complex chemical systems with overlapping spectral bands.

Figure 1 shows three different transient absorption images taken at a total P = 10 Torr in the presence of ~5% molecular oxygen, ([O$_2$] = 1.65·10^{16}cm^{-3}). The image in Fig. 1A was acquired under "baseline" conditions, i.e. only the radical precursor (CH$_3$CHI$_2$) and O$_2$ were diluted in the He bath. Figures 1B and 1C display the transient signals with addition of SO$_2$ ([SO$_2$] = 4.7·10^{13}cm^{-3}) and water vapor ([H$_2$O] = 1·10^{17}cm^{-3}), respectively. The false-color scale indicates absorption intensity; kinetic time t = 0 marks the arrival of the photolysis laser pulse. At first glance, two main spectral features are apparent in Fig. 1: a strong, broad absorption band centered at ~340 nm and a weaker structured band at longer wavelengths. However, a careful examination of the time-resolved spectra in Fig. 1C reveals that the intense 340-nm absorption actually consists of two spectral contributions: a high-energy component centered at ~325 nm and a low-energy component that extends to longer wavelengths (labelled

Band I and Band II, respectively). All of the transient signals appear promptly after photolysis, indicating that they arise from reactions in Scheme 2. Bands I and II decay with timescales that depend on SO$_2$ and H$_2$O. In contrast, the weaker, structured absorption at longer wavelengths persists throughout the experimental observation window, unaffected by either SO$_2$ or water.

Based on the transient spectra at long kinetic times averaged over t = 4 – 5 ms (Fig. S1, ESI), we can easily identify the long-lived spectral feature as the absorption spectrum of IO,[29] which is formed mostly by secondary chemistry in reactions of iodoalkyl radicals with O$_2$.[30] Under our conditions, IO does not decay on the experimental timescale because it is not reactive towards SO$_2$ or H$_2$O. The other dominant transient signal evident in the long-time spectra is the photolytic depletion of CH$_3$CHI$_2$. The IO absorption and precursor depletion signals can be easily subtracted from the transient absorption measurements in order to focus solely on the contributions of Bands I and II (see ESI).

A quantitative analysis of the experimental measurements in Fig. 1C (in the presence of H$_2$O) is given in Fig. 2. Panel 2A shows the time evolution of the absorption signals averaged over the λ = 320 – 400 nm range. The data fit successfully to a kinetic model made up of two independent components, each with a single exponential rise and decay. These two fit components, shown individually in Fig. 2A, decay with first-order rates (1/τ$_{decay}$) of 2800±300 s^{-1} and 175±25 s^{-1}. All errors reported throughout this report are 1σ, and details of the fits and the error treatment are provided in the ESI. To separate the spectra of the two species that give rise to these decay timescales we average the absorption signals between t = 1 – 2 ms. This yields the spectrum of only the slowly decaying component (Band I in Fig. 1C). The long-lived spectrum of Band I can then be appropriately scaled and subtracted from the total transient spectrum, resulting in the spectrum of only the short-lived component, labelled Band II. The two spectra are plotted in Fig. 2B, extrapolated to their fitted intensities at t = 0. In a complementary approach (see ESI), we fit absorption traces at different probe wavelengths to the same kinetic model. The amplitudes of Bands I and II obtained in this way are entirely consistent with the spectra in Fig. 2B, which supports our conclusion: the broad 340-nm absorption band in Fig. 1 consists of two independent species with differing reactivity towards H$_2$O.

The slowly-decaying spectrum of Band I is nearly identical to the UV spectrum of *syn*-CH$_3$CHOO, measured recently by Smith *et al.* in a combined direct absorption and photoionization depletion study.[20] Because of this similarity we assign Band I to the
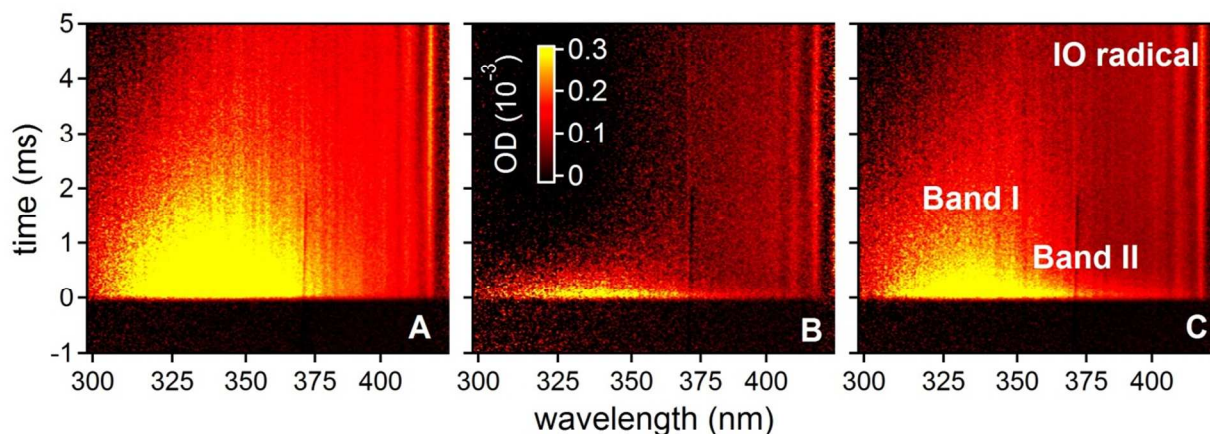

Fig. 1 Transient absorption images of the reaction CH$_3$CHI + O$_2$ in He buffer gas with [O$_2$] = 1.65·10^{16}cm^{-3}, total P = 10 Torr. The false-color scale indicates absorbance per single cavity pass. *Panel A:* [SO$_2$] = 0, [H$_2$O] = 0. *Panel B:* [SO$_2$] = 4.7·10^{13}cm^{-3}, [H$_2$O] = 0. *Panel C:* [SO$_2$] = 0, [H$_2$O] = 1·10^{17}cm^{-3}
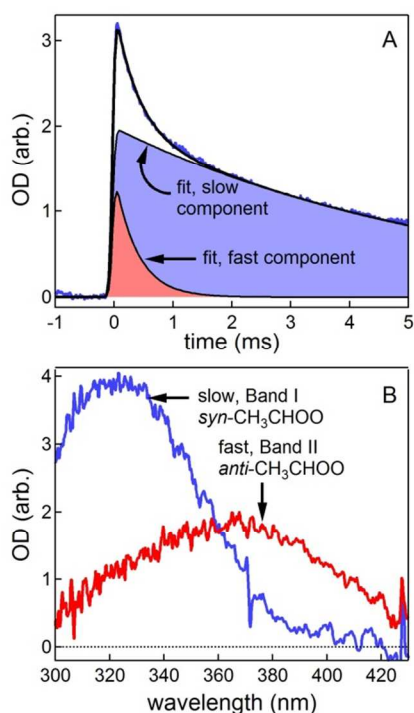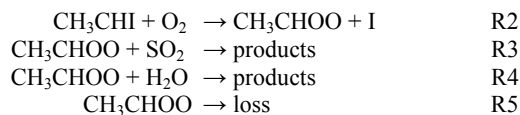
Fig. 2 *Panel A:* Transient absorption in the presence of H_2O (from Fig. 1C), averaged over $\lambda = 320 - 400$ nm. Thick black line is a fit to two components, shown separately by blue and red shaded areas. *Panel B:* UV spectra of the two kinetic components, extrapolated to $t = 0$.
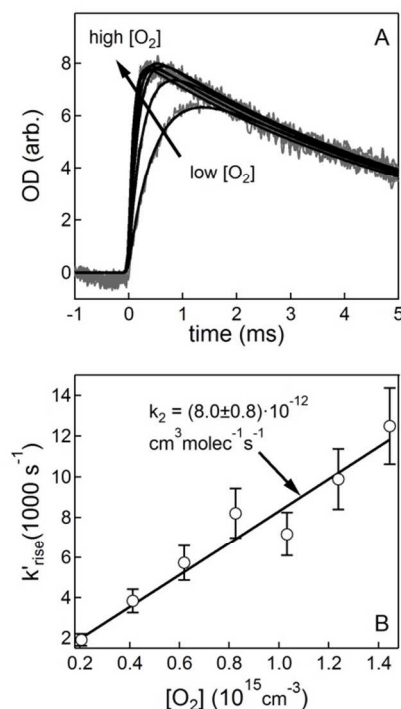

Fig. 3 *Panel A:* Transient absorption traces at varying $[O_2]$, averaged over $\lambda = 320 - 400$ nm, in the absence of SO_2 or H_2O. Black lines are kinetic fits. *Panel B:* Determination of the bimolecular rate coefficient k_2 for the reaction $CH_3CHI + O_2$ from pseudo–first-order decay rates, k_2'.

$B(^1A') \leftarrow X(^1A')$ electronic transition of *syn*-CH_3CHOO. Band II, on the other hand, has not been reported before, but several observations indicate that it is due to the *anti*-CH_3CHOO isomer. First, the appearance timescale of Bands I and II is the same (see below), which is consistent with our expectation that *syn*- and *anti*-CH_3CHOO are formed in the same reaction (R2, Scheme 2). Second, it is unlikely that any other species give rise to Band II absorption. In analogy to the case of CH_2OO, reaction R2 may produce some acetaldehyde + IO along with stabilized CH_3CHIO_2 radicals. Yet, the UV spectrum of acetaldehyde[31] does not match Band II; CH_3CHIO_2 should be a minor product with moderate absorption cross-section (analogous to CH_2IO_2) and should not contribute significantly to our transient signal either. Third, the species responsible for Band II reacts with water vapor (see below) with a rate coefficient consistent with calculations and with prior measurements of *anti*-CH_3CHOO. Lastly, Band II is red-shifted from *syn*-CH_3CHOO absorption, as predicted by calculations of the *anti*-CH_3CHOO spectrum.[18,20]
We interpret our isomer-resolved measurements of the formation and decay kinetics of CH_3CHOO in the context of the following mechanism:

$$
\begin{aligned}
CH_3CHI + O_2 &\rightarrow CH_3CHOO + I & \text{R2} \\
CH_3CHOO + SO_2 &\rightarrow products & \text{R3} \\
CH_3CHOO + H_2O &\rightarrow products & \text{R4} \\
CH_3CHOO &\rightarrow loss & \text{R5}
\end{aligned}
$$

Reaction R5 includes all first-order removal processes such as wall loss or unimolecular decomposition. Based on analogy with CH_2OO, the self-reaction of CH_3CHOO may be very fast,[27,32] and indeed our measurements at high initial radical concentrations revealed non-exponential signal decays. Because of this, we reduced the initial CH_3CHI concentration to $\sim 7 \cdot 10^{11}$ cm^{-3}. Tests of various kinetic fit functions showed that at these conditions the experimental signals no
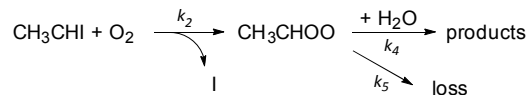
longer showed signs of second-order decays, meaning that self-reaction of CH_3CHOO was effectively supressed.
Figure 3 shows the $[O_2]$-dependence of the transient absorption with no H_2O or SO_2. The data, averaged over $\lambda = 320 - 400$ nm, are fit to a single exponential rise and decay (see ESI), describing a simplified kinetic model with only one formation and removal pathway:

$$CH_3CHI + O_2 \xrightarrow{k_2} CH_3CHOO \xrightarrow{k_5} loss$$
$$\downarrow$$
$$I$$
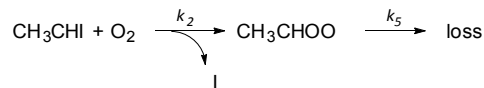
The decay of CH_3CHOO absorption (reaction R5) is not sensitive to the oxygen concentration, whereas its formation is governed by the reaction R2. A plot of the inverse of the signal rise time ($1/\tau_{rise}$) vs. $[O_2]$ yields the rate coefficient $k_2 = (8.0 \pm 0.8) \cdot 10^{-12}$ cm^3 s^{-1}, a factor of ~ 5 higher than for the analogous case of $CH_2I + O_2$.[14,33] Notably, fitting of data at different probe wavelengths (see ESI) shows that the rise and decay times of Bands I and II are the same, consistent with *syn*- and *anti*-CH_3CHOO being formed together.
Figure 4A shows selected transient absorption traces at a constant $[O_2] = 1.65 \cdot 10^{16}$ cm^{-3} and at varying $[H_2O]$, along with fits to a model (see ESI) that describes the reactions:

$$CH_3CHI + O_2 \xrightarrow{k_2} CH_3CHOO \xrightarrow[k_4]{+ H_2O} products$$
$$\downarrow \qquad\qquad \searrow^{k_5}$$
$$I \qquad\qquad\qquad loss$$

The fit function is a sum of two kinetic components, each with single exponential rise and decay. We fix the rise times at 132,000 s^{-1} based on our determination of k_2, but allow the decay times for each component to vary. Panel 4B shows that the decay rate of *syn*-CH_3CHOO does not change as a function of $[H_2O]$ from its baseline value of 160 ± 25 s^{-1}, most likely limited by loss through diffusion out of the probe volume. Consequently, we can only obtain an upper
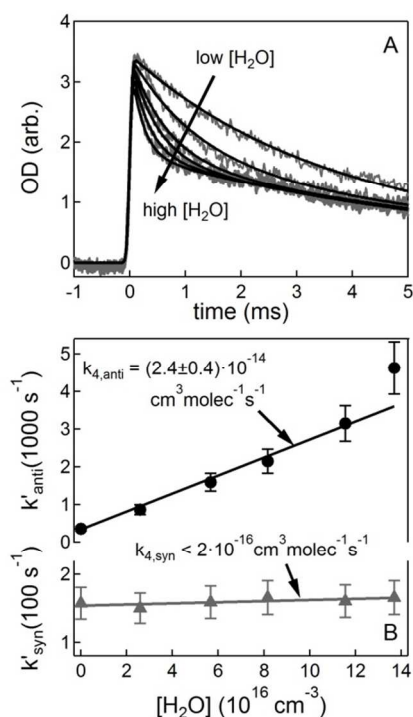
Fig. 4 *Panel A:* Transient signals at varying [H_2O], averaged over $\lambda = 340 - 380$ nm. Black lines are kinetic fits. *Panel B:* Determination of conformer-specific rate coefficients $k_{4,syn}$ and $k_{4,anti}$ from pseudo–first-order decay rates, k_4'.

limit for $k_{4,syn} < 2 \cdot 10^{-16}$ cm^3 s^{-1}. This result agrees with calculations by Anglada *et al.*[2] ($2.39 \cdot 10^{-18}$ cm^3 s^{-1}) and with the experimentally derived upper limit ($k_{4,syn} < 4 \cdot 10^{-15}$ cm^3 s^{-1}) by Taatjes *et al.*[23].

In contrast, *anti*-CH_3CHOO decay rate increases linearly with [H_2O], which allows a determination of the bimolecular rate coefficient, $k_{4,anti} = (2.4\pm0.4) \cdot 10^{-14}$ cm^3 s^{-1}. It is 7 times lower that the high-pressure limiting value by Anglada *et al.*[2] and 2.4 times higher than the results of Taatjes *et al.*[23] The large (over two orders of magnitude) difference between the rate coefficients for *syn*- and *anti*-CH_3CHOO + H_2O is in agreement with the predicted lower reaction barrier for the *anti*- conformer.

The absorption signals also show biexponential decays in the presence of SO_2, but the difference between the two CH_3CHOO isomers is less pronounced than in the reaction with H_2O. The plots of the pseudo-first-order decay rates as a function of [SO_2] are shown in Fig. 5. The rate coefficient for *syn*-CH_3CHOO + SO_2 is $k_{3,syn} = (2.9\pm0.3) \cdot 10^{-11}$ cm^3 s^{-1}, in good agreement with the findings by Taatjes *et al.*[23] of $(2.4\pm0.3) \cdot 10^{-11}$ cm^3 s^{-1}. In the case of the *anti*-conformer we determine $k_{3,anti} = (2.2\pm0.2) \cdot 10^{-10}$ cm^3 s^{-1}, which is a factor of ~3 higher than that obtained by Taatjes *et al.*[23] The systematic differences between our reaction rate coefficients for *anti*-CH_3CHOO and those found by PIMS detection is probably due to better sensitivity and selectivity afforded by UV spectroscopic probing for this chemical system.

The UV spectrum of *syn*-CH_3CHOO described here is centered at 323 nm (~3.8 eV) and is ~40 nm wide (FWHM). It is substantially broader than that reported by Beames *et al.*[18] using photoionization depletion measurements under molecular beam conditions. This discrepancy, which is similar to the case of CH_2OO UV spectrum,[14] may arise from the differences in detection technique or from the dissimilar temperatures in our flow reactor and in the cold molecular jet of Beames *et al.* Our results agree overall with those reported by
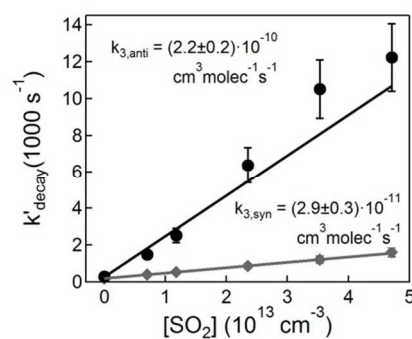

Fig. 5 Determination of isomer-specific rate coefficients for the reaction $CH_3CHOO + SO_2$ ($k_{3,syn}$, $k_{3,anti}$) from pseudo–first-order decay rates k_3'.

Smith *et al.*;[20] however, our *syn*-CH_3CHOO spectrum is less intense than theirs on the low-energy side. When the spectra are scaled to match their maximum intensities (see ESI), the spectrum of Smith *et al.* resembles the sum of transient absorptions of Bands I and II in our study, which suggests that their results may in fact contain unresolved contributions from both CH_3CHOO isomers.

The UV spectrum of *anti*-CH_3CHOO is centered at ~360 nm (~3.4 eV) and has a width of ~55 nm. The roughly 0.4 eV shift in the band maximum compares well to the calculated shifts of ~0.3 eV by Beames *et al.*[18] and ~0.35 eV by Smith *et al.*[20] This agreement supports the theoretical prediction that the B state is destabilized relative to the ground state more strongly for *syn*-CH_3CHOO than for *anti*-CH_3CHOO because of the electronic interaction of the methyl and the carbonyl oxide groups.[18]

Without knowledge of the *syn*-/*anti*-CH_3CHOO branching ratio in reaction R2 we cannot determine their UV cross-sections directly. However, Smith *et al.*[20] report the absolute UV cross-section of $1.06 \cdot 10^{-17}$ cm^2 for CH_3CHOO by ion depletion measurements at 308 nm, where only the *syn*- isomer contributes significantly. Scaling our UV spectrum to that value, the peak absorption cross-section of *syn*-CH_3CHOO at 323 nm is $1.2 \cdot 10^{-17}$ cm^2, and its initial concentration in our experiments is $4.2 \cdot 10^{11}$ cm^{-3}. Photodissociation of CH_3CHI_2 produces ~$6.7 \cdot 10^{11}$ cm^{-3} radicals at these conditions, and our transient spectra reveal prompt formation of ~$0.7 \cdot 10^{11}$ cm^{-3} of IO (see ESI). Since there are no other major products in reaction R2, we infer that the initial concentration of *anti*-CH_3CHOO is ~$1.8 \cdot 10^{11}$ cm^{-3}, or about ~30% of the total CH_3CHOO that is produced. This yield of *anti*-CH_3CHOO is greater than estimated previously.[23] *Anti*-CH_3CHOO is computed to be less stable than the *syn*- conformer by ~3.5 kcal/mol,[2] so its yield of almost 1/3 might at first seem surprising. However, the decomposition of the activated CH_3CHIO_2 complex may form a non-thermal product distribution and generate more *anti*-CH_3CHOO than would be expected based purely on thermochemistry. Once formed, the two conformers will not interconvert because of the large gas-phase barrier to isomerization (>20 kcal/mol).[2]

Using our estimate of the initial *anti*-CH_3CHOO concentration, its peak cross-section at ~360 nm is $1.2 \cdot 10^{-17}$ cm^2, which is very similar to the peak cross-section of the *syn*-conformer. Given the greater width of the *anti*-CH_3CHOO spectrum, its oscillator strength is slightly larger than that of *syn*-CH_3CHOO, in agreement with the calculations of Smith *et al.*[20] Due to the assumptions involved in our analysis, we treat our derivation of the *anti*-CH_3CHOO UV cross-section as a qualitative guide and expect it to be correct to within a factor of 2. A convolution of the *anti*-CH_3CHOO UV absorption cross-section with the solar actinic flux (see ESI) allows an estimate of the photolytic lifetime of *anti*-CH_3CHOO in the atmosphere,

similar to the treatment of *syn*-CH₃CHOO by Smith *et al.*[20] At sea level the lifetime of *anti*-CH₃CHOO varies from 3.8 to 6.6 s for solar zenith angles of 0 - 60°, respectively. This is slightly less than the lifetime of the *syn*- conformer due to the better overlap of the red-shifted *anti*-CH₃CHOO absorption band with the solar flux spectrum. For both isomers of acetaldehyde oxide, photochemical destruction is too slow to compete with reactive removal by atmospheric species such as H_2O, SO_2, and NO_x.

Conclusions

In conclusion, we present the UV absorption spectra of the two conformers of acetaldehyde oxide, *syn*- and *anti*- CH₃CHOO. The spectrum of *syn*-CH₃CHOO agrees well with another recent spectroscopic study of this species by Smith *et al*. Aided by comparison with their results, we determine the *syn*-/*anti* branching ratio to be approximately 3:1 in a low-pressure bath of 10 Torr He at 293K. The peak absorption cross-section of *anti*-CH₃CHOO is comparable to that of the *syn*-conformer, but the band maximum is shifted to lower energy by ~0.4 eV. This band shift slightly increases the solar photolysis rate of *anti*-CH₃CHOO in the atmosphere compared to *syn*-CH₃HCOO, although the primary removal mechanism for both conformers is the reaction with other trace atmospheric species.

UV probing of the reaction kinetics of CH₃CHOO with SO_2 and H_2O shows conformer-dependent behavior, in agreement with theoretical predictions and prior experiments. Most importantly, knowledge of the UV absorption spectra of the two conformers of CH₃CHOO expands our capabilities for direct experimental measurements of CI reactivity using the simple and widely available technique of time-resolved UV spectroscopy.

Acknowledgements

Notes and references

[a] Combustion Research Facility, MS 9055, Sandia National Laboratories, Livermore, CA, 94551-0969, USA

[b] Department of Chemistry, Saint Michael's College, Colchester, VT, 05439, USA.

† Electronic Supplementary Information (ESI) available: experimental setup, kinetic models and fitting, solar lifetime calculations.

1. R. Criegee, *Angew. Chem., Int. Ed. Engl.*, 1975, **14**, 745-752.
2. J. M. Anglada, J. Gonzalez and M. Torrent-Sucarrat, *Phys. Chem. Chem. Phys.*, 2011, **13**, 13034-13045.
3. D. Johnson and G. Marston, *Chem. Soc. Rev.*, 2008, **37**, 699-716.
4. L. Vereecken and J. S. Francisco, *Chem. Soc. Rev.*, 2012, **41**, 6259-6293.
5. L. Vereecken, H. Harder and A. Novelli, *Phys. Chem. Chem. Phys.*, 2012, **14**, 14682-14695.
6. N. M. Donahue, G. T. Drozd, S. A. Epstein, A. A. Presto and J. H. Kroll, *Phys. Chem. Chem. Phys.*, 2011, **13**, 10848-10857.
7. O. Horie and G. K. Moortgat, *Acc. Chem. Res.*, 1998, **31**, 387-396.
8. C. A. Taatjes, D. E. Shallcross and C. J. Percival, *Phys. Chem. Chem. Phys.*, 2014, **16**, 1704 - 1718.
9. C. A. Taatjes, G. Meloni, T. M. Selby, A. J. Trevitt, D. L. Osborn, C. J. Percival and D. E. Shallcross, *J. Am. Chem. Soc.*, 2008, **130**, 11883-11885.
10. O. Welz, J. D. Savee, D. L. Osborn, S. S. Vasu, C. J. Percival, D. E. Shallcross and C. A. Taatjes, *Science*, 2012, **335**, 204-207.
11. M. Nakajima and Y. Endo, *J. Chem. Phys.*, 2013, **139**, 101103.
12. Y. T. Su, Y. H. Huang, H. A. Witek and Y. P. Lee, *Science*, 2013, **340**, 174-176.
13. J. M. Beames, F. Liu, L. Lu and M. I. Lester, *J. Am. Chem. Soc.*, 2012, **134**, 20045-20048.
14. L. Sheps, *The Journal of Physical Chemistry Letters*, 2013, **4**, 4201-4205.
15. W.-L. Ting, Y.-H. Chen, W. Chao, M. C. Smith and J. J.-M. Lin, *Phys. Chem. Chem. Phys.*, 2014, **16**, 10438-10443.
16. J. H. Lehman, H. Li, J. M. Beames and M. I. Lester, *The Journal of chemical physics*, 2013, **139**, 141103.
17. J. Li, S. Carter, J. M. Bowman, R. Dawes, D. Xie and H. Guo, *The Journal of Physical Chemistry Letters*, 2014, **5**, 2364-2369.
18. J. M. Beames, F. Liu, L. Lu and M. I. Lester, *J. Chem. Phys.*, 2013, **138**, 244307.
19. F. Liu, J. M. Beames, A. M. Green and M. I. Lester, *The Journal of Physical Chemistry A*, 2014.
20. M. C. Smith, W.-L. Ting, C.-H. Chang, K. Takahashi, K. A. Boering and J. J.-M. Lin, *The Journal of chemical physics*, 2014, **141**, 074302.
21. M. Nakajima and Y. Endo, *The Journal of chemical physics*, 2014, **140**, 011101.
22. C. A. Taatjes, O. Welz, A. J. Eskola, J. D. Savee, D. L. Osborn, E. P. F. Lee, J. M. Dyke, D. W. K. Mok, D. E. Shallcross and C. J. Percival, *Phys. Chem. Chem. Phys.*, 2012, **14**, 10391-10400.
23. C. A. Taatjes, O. Welz, A. J. Eskola, J. D. Savee, A. M. Scheer, D. E. Shallcross, B. Rotavera, E. P. F. Lee, J. M. Dyke, D. K. W. Mok, D. L. Osborn and C. J. Percival, *Science*, 2013, **340**, 177-180.
24. Y. Liu, K. D. Bayes and S. P. Sander, *The Journal of Physical Chemistry A*, 2014, **118**, 741-747.
25. D. Stone, M. Blitz, L. Daubney, N. U. Howes and P. Seakins, *Phys. Chem. Chem. Phys.*, 2014, **16**, 1139-1149.
26. O. Welz, A. J. Eskola, L. Sheps, B. Rotavera, J. D. Savee, A. M. Scheer, D. L. Osborn, D. Lowe, A. Murray Booth and P. Xiao, *Angew. Chem.*, 2014, **126**, 4635-4638.
27. Z. J. Buras, R. M. Elsamra and W. H. Green, *The Journal of Physical Chemistry Letters*, 2014, **5**, 2224-2228.
28. L. Vereecken, H. Harder and A. Novelli, *Phys. Chem. Chem. Phys.*, 2014, **16**, 4039-4049.
29. M. H. Harwood, J. B. Burkholder, M. Hunter, R. W. Fox and A. R. Ravishankara, *J. Phys. Chem. A*, 1997, **101**, 853-863.
30. T. J. Gravestock, M. A. Blitz, W. J. Bloss and D. E. Heard, *ChemPhysChem*, 2010, **11**, 3928-3941.
31. R. D. Martinez, A. A. Buitrago, N. W. Howell, C. H. Hearn and J. A. Joens, *Atmospheric Environment. Part A. General Topics*, 1992, **26**, 785-792.
32. W.-L. Ting, C.-H. Chang, Y.-F. Lee, H. Matsui, Y.-P. Lee and J. J.-M. Lin, *The Journal of chemical physics*, 2014, **141**, 104308.
33. D. Stone, M. A. Blitz, L. Daubney, T. Ingham and P. W. Seakins, *Phys. Chem. Chem. Phys.*, 2013, **15**, 19119.